3 One-dimensional sediment modelling: excavation, infill and collapse

3.1 *Introduction*

Diffusion models are commonly used to model the transport of solid species in sediment, despite the fact that the drawbacks of this approach are well known. Over 15 years ago, Boudreau (1986a) showed that the diffusion analogy is appropriate under only very specific circumstances: the mixing needs to be rapid relative to the tracer decay rate, and the transport distances need to be small relative to the size of the mixing layer and the scale of the profile. Boudreau (1986b) developed a general model framework that allows the construction of any number of more physically realistic 'non-local' models.

Non-local models include variations on the conveyor belt model theme (eg. Robbins (1986), Boudreau (1986b)), and less commonly regenerator or burrow-and-fill models (eg. Gardner et al. (1987), Sharmer et al. (1987)). Transition matrix approaches (discussed in Section 1.2.3) are another form of discrete non-local model, and have been used in several studies (eg. Foster (1985), Trauth (1998), Shull (2001) and Shull and Yasuda (2001)). All these models have the advantage that they are firmly linked to measurable physical processes (eg. worm feeding and excretion rates and depths), as opposed to a biodiffusion coefficient.

My laboratory measurements of thalassinidean shrimp sediment transport (Chapter 2) demonstrated rapid excavation of sediment from depth, and considerable downward transport of surface material back into the burrow. A diffusion model would be quite inappropriate for modelling these sediment transport processes, and in this chapter I propose a non-local model which is a hybrid between a conveyor belt and burrow-and-fill model (Boudreau (1997)). I refer to it as the EIC model (Excavate, Infill and Collapse).

One view that I've encountered during my work is that a more complicated description of bioturbation is unnecessary since the diffusion model is not over-parameterised and it usually gives a good fit to the data. A more realistic transport process description is desirable if the aim is to overlay sediment diagenesis reactions onto the transport model. In practice, getting the data for a more physically realistic transport process is rarely possible. For example, Boudreau (1986a) concluded 'For isotopes outside the window of sensitive parameter values, the data may never be of sufficient accuracy to warrant the use of realistic but more complex mixing functions'.

In this chapter I demonstrate that the EIC model can be applied with the same ease as a diffusion model and can produce very similarly shaped profiles. Its value may be in testing diagenesis model results. The same diagenesis model could be executed with two very different underlying transport assumptions to see whether results differ significantly. Further significant advantages of the EIC model are that the parameters can be linked to measurable quantities, and that it can be readily expanded into two or three dimensions (discussed in Chapter 4).

3.2 *Model derivation*

Boudreau (1986b) described a general one dimensional model that allows descriptions of bioturbation at a range of scales. Diffusion, conveyor belt, burrow-and-fill (or regenerator) models and many other bioturbation models can be derived from the general equation (Boudreau (1986b), Boudreau and Imboden (1987)). The tracer conservation equation allows for transport between different locations within the sediment column, and for exchange across the sediment water interface:

$$
\begin{aligned}
\frac{\partial \phi_s(z,t)p(z,t)}{\partial t} &= \int_0^{L_2} \phi_s(z',t)K(z',z;t)p(z',t)dz' && \text{---- transport to z from elsewhere in the sediment column;} \\
&+K_I(z,t)f_p(t) && \text{---- injection of material at z from the overlying water column;} \\
&-\phi_s(z,t)p(z,t)\int_0^{L_1} K(z,z';t)dz' && \text{---- removal from z to elsewhere in the sediment column;} \\
&-\phi_s(z,t)p(z,t)K_E(z,t) && \text{---- removal from z to the overlying water column;} \\
&-\frac{\partial \phi_s(z,t)w(z,t)p(z,t)}{\partial z} && \text{---- transport by advection} \\
&+R(z,t,p(z,t)) && \text{---- production or decay}
\end{aligned}
\qquad \textbf{(3.1)}
$$

where ϕ_s is the solid fraction ($\phi_s = 1-\phi$, where ϕ is porosity), p(z,t) is the property of interest (eg. tracer concentration), t is time, $K(z,z';t)$ is the fraction of material removed from depth z per unit depth and per unit time and transported to depth z', $K_I(z,t)$ is the fraction of the external flux injected per unit depth in the sediment, $f_p(t)$ is the external flux of the property of interest (units of property mass per unit area and time), $K_E(z,t)$ is the fraction of material removed from depth z and transported to the water column per unit time, R is the rate of production or decay due to chemical reaction or radioactivity, L_2 is the deepest position of material delivery and L_1 is the deepest point of material removal.

For burrowing animals such as thalassinidean shrimp, I have assumed that the dominant transport processes are: burrow excavation (material transported from depth to the surface), burrow infill (surface material dropping down a burrow shaft and filling the burrow) and burrow collapse (material directly above a burrow tunnel shifting downwards to close the tunnel). The EIC model is a one-dimensional description of these processes derived from equation (3.1). Only four terms in equation (3.1) have been used: removal from depth to the overlying water column, transport to depth from elsewhere in the sediment column, transport by advection, and the reaction term. The model is split into two layers so that a uniformly mixed surface layer of thickness z_r overlies a region containing burrows extending to depth L. It is assumed that the surface layer is mixed rapidly due to waves, and surface dwelling animals. The lower region loses material to the surface (burrow excavation) and receives well-mixed material back from the surface layer (burrow infill) and from the sediment directly above the burrow structures (burrow collapse). In other words, burrowed material is transported to the surface and the resulting burrow void is refilled with either surface sediment, sediment collapsed from above or a mixture of the two. There is no diffusive mixing. Diagrams representing the model assumptions are given in Figure 3.1.

Removal from the lower layer is described by a removal function $K_E(z)$ (the fraction of sediment volume removed at depth z per unit time, units of time^{-1}). The excavated material returns to the sediment column via the sediment surface, and is characterised by a surface flux boundary condition in the model. The burrows immediately receive uniformly mixed surface material. In Boudreau's burrow and fill model (Boudreau and Imboden (1987)), the burrows are filled completely through infill. In the EIC model, the extent to which the burrow is filled is set by a parameter, f whose values lie between 0 and 1. When $f = 1$, the burrow is completely filled with surface material and there is no burrow collapse. When $f = 0$, no surface material fills the burrow and the burrow cavity closes due to collapse. Intermediate values represent a combination of infill and burrow collapse.

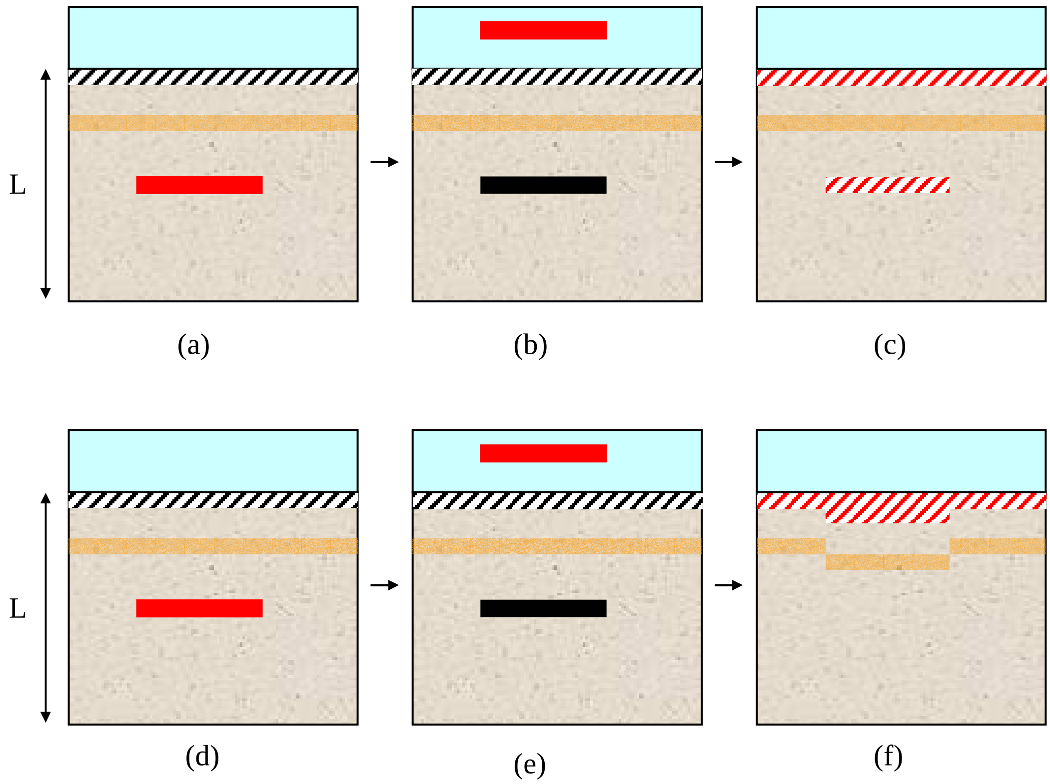

Figure 3.1 An idealised representation of infill-only ((a), (b) and (c)) and collapse-only ((d), (e) and (f)) burrowing scenarios, with zero sedimentation velocity. The uniformly-mixed surface layer is represented by a diagonal-striped pattern. In both cases, a burrow is excavated from a horizontal tunnel at depth (red rectangle of sediment in (a) and (d)). The excavated material is removed from the sediment column to the overlying water leaving a void at depth (black rectangle in (b) and (e)). The excavated material is deposited on the surface and uniformly mixed through the surface layer (change represented by shift from black to red diagonal stripes, indicating that excavated material has been included in the surface layer). The void is filled either with surface sediment only (infill, (c)), sediment directly above the void only (collapse, (f)) or a mixture of the two (not illustrated). In this chapter the EIC model is one-dimensional and assumes a uniform burrowing rate with depth. This diagram represents non-uniform burrowing in two dimensions for ease of conceptualisation only.

The four terms from equation (3.1) used in the derivation of the EIC model are as follows.

$\int_0^{L_2} \phi_s(z',t)K(z',z;t)p(z',t)dz'$ represents transport from elsewhere in the sediment column. This term captures the transport from the surface layer ($z^* < z_r^*$) to the burrowing zone ($z_r^* < z^* < 1$).

$\phi_s(z,t)p(z,t)K_E(z,t)$ is removal of material from location z to the overlying water column. In other words, I assume that the material excavated in the burrowing process is pumped to the water column and its return to the sediment surface is represented by a flux boundary condition (described later).

$\frac{\partial \phi_s(z,t) w(z,t) p(z,t)}{\partial z}$ represents transport by advection.

$R(z,t,p(z,t))$ is the reaction/production term.

Putting these terms together yields:

$$\frac{\partial \phi_s(z,t) p(z,t)}{\partial t} = \int_0^{L_2} \phi_s(z',t) K(z',z;t) p(z',t)\,\mathrm{d}z' - \phi_s(z,t) p(z,t) K_E(z,t) - \frac{\partial \phi_s(z,t) w(z,t) p(z,t)}{\partial z} + R(z,t,p(z,t)) \quad \textbf{(3.2)}$$

$K(z',z;t)p(z',t)$ is the fraction of material removed from depth z' per unit depth and per unit time and transported to z. In the EIC model K is zero if $z' > z_r$ (no material is moved from the burrowing zone to elsewhere in the sediment column, other than by advection, as all excavated material is expelled to the water column). Material is taken from the surface mixed layer ($z' < z_r$) and distributed over a range of z, by a function defined here as

$$K(z',z;t) = \begin{cases} a_s s_f(z) & \text{if } z' < z_r \\ 0 & \text{if } z' > z_r \end{cases} \quad \textbf{(3.3)}$$

where a_s is a constant and $s_f(z)$ is a distribution function defined so that $\int_0^L s_f(z)\,\mathrm{d}z = 1$.

Now substituting in the definition for K and setting $\phi_\sigma(z) = \phi_{s1}$ and $p(z) = p_1$ when $z < z_r$ (both constants because the surface layer has uniform properties) the first term of equation (3.2) becomes:

$$\begin{aligned} \int_0^L \phi_s(z',t) K(z',z;t) p(z',t)\,\mathrm{d}z' &= \int_0^{z_r} \phi_s(z',t) a_s s_f(z) p(z',t)\,\mathrm{d}z' \\ &= \phi_{s1} p_1 a_s z_r s_f(z) \end{aligned} \quad \textbf{(3.4)}$$

So we now have:

$$\frac{\partial \phi_s(z,t) p(z,t)}{\partial t} = \phi_{s1} p_1 a_s z_r s_f(z) - \phi_s(z,t) p(z,t) K_E(z,t) - \frac{\partial \phi_s(z,t) w(z,t) p(z,t)}{\partial z} + R(z,t,p(z,t)) \quad \textbf{(3.5)}$$

The next assumption is that the volume returned to the burrow per unit time cannot exceed the volume excavated from the burrow per unit time. The excavated volume per unit time is:

$$\int_0^L K_E \, \mathrm{d}z = K_{\mathrm{av}} L \tag{3.6}$$

so K_{av} (dimension time^{-1}) is defined to be the depth-averaged excavation rate over the sediment column. The fraction of this excavated volume that is returned as burrow infill is denoted f, so the infill volume per unit time is $fK_{av}L$.

Using equation (3.5) and substituting the sediment density ρ_s for p, the mass of solid infill is $\int_0^L \phi_{s1} z_r a_s \rho_s s_f(z) \mathrm{d}z = \phi_{s1}\rho_s a_s z_r$ and the bulk density of the solid infill is $\phi_s\rho_s$, so the volume of solid infill is $z_r a_s$.

Thus we infer that $z_r a_s = fK_{\mathrm{av}}L$ and so

$$\frac{\partial \phi_s(z,t)p(z,t)}{\partial t} = \phi_{s1}p_1 fK_{av}Ls_f(z) - \phi_s(z,t)p(z,t)K_E(z,t) - \frac{\partial \phi_s(z,t)w(z,t)p(z,t)}{\partial z} + R(z,t,p(z,t)) \tag{3.7}$$

The lower layer equations for total solids and tracer concentration are then:

$$\frac{\partial \phi_s}{\partial t} = s_f(z) fK_{av}L\phi_{s1} - K_E(z)\phi_s - \frac{\partial w\phi_s}{\partial z} \tag{3.8}$$

$$\frac{\partial \phi_s C}{\partial t} = s_f(z) fK_{av}L\phi_{s1}C_1 - K_E(z)\phi_s C - \frac{\partial w\phi_s C}{\partial z} - \lambda\phi_s C \tag{3.9}$$

where λ is the decay constant for the tracer, C is the concentration of the tracer (mass per unit volume of solids), C_1 is the tracer concentration in the surface layer and ϕ_{s1} is the solid fraction in the surface layer. The terms on the right hand side of equation (3.9) represent infill, excavation, advection and decay (from left to right respectively).

The surface layer equations for total solids and for tracer concentration are:

$$\frac{\mathrm{d}\phi_{s1}}{\mathrm{d}t} = \frac{w_0\phi_{s0} - w_r\phi_{s1} - \phi_{s1}fK_{av}L\int_{z_r}^{L} s_f(z)\,\mathrm{d}z}{z_r} = \frac{w_0\phi_{s0} - w_r\phi_{s1} - \phi_{s1}fK_{av}L}{z_r} \tag{3.10}$$

$$\frac{\mathrm{d}\phi_{s1}C_1}{\mathrm{d}t} = \frac{w_0\phi_{s0}C_0 - w_r\phi_{s1}C_1 - \phi_{s1}C_1fK_{av}L\int_{z_r}^{L} s_f(z)\,\mathrm{d}z}{z_r} - \lambda\phi_{s1}C_1 = \frac{w_0\phi_{s0}C_0 - w_r\phi_{s1}C_1 - \phi_{s1}C_1fK_{av}L}{z_r} - \lambda\phi_{s1}C_1 \tag{3.11}$$

where ϕ_{s0} and C_0 are the solid fraction and tracer concentration of the material arriving at the sediment water interface, w_r is the velocity at the base of the surface mixed layer. w_0 is the velocity at the sediment water interface, and is comprised of the sedimentation velocity (w_E) and the excavated material being returned to the sediment via the sediment surface. The flux boundary conditions at the sediment surface are:

$$\phi_{s0}w_0 = \phi_{sE}w_E + \int_{z_r}^{L} \phi_s K_E(z)\,\mathrm{d}z \tag{3.12}$$

$$\phi_{s0}w_0C_0 = \phi_{sE}F_{in} + \int_{z_r}^{L} \phi_s K_E(z)C\,\mathrm{d}z \tag{3.13}$$

where ϕ_{sE} is the solid fraction of sedimenting material and $\phi_{sE}F_{in}$ is the concentration flux of material arriving at the sediment water interface from the water column. The terms on the right hand side of each equation represent the fluxes to the surface due to sedimentation and excavation respectively. Note that $\phi_{sE}F_{in}$ could be represented as $\phi_{sE}w_EC_E$ (where C_E is the concentration of incoming material), however I wanted to be able to model finite concentration fluxes with zero volume flux.

Boudreau (1986a) non-dimensionalised equations before further analysis. Non-dimensionalisation simplifies the analysis somewhat and allows the identification of important parameter combinations. Characteristic length, concentration flux and time scales have been chosen from L, F_{in} and K_{av} respectively. Note that Boudreau (1986a) used L/w as a characteristic time scale, which presents difficulties if dealing with a system with zero sedimentation velocity. A more meaningful measure in cases where sedimentation velocity is negligible is to normalise quantities against a measure of the excavation rate, K_{av}. Boudreau used the tracer concentration of the sedimenting material to normalise tracer concentration. Here I have normalised by the incoming concentration flux to allow for the possibility that there may be a negligible volume flux ($w_E = 0$) but significant concentration flux to the surface.

The non-dimensionalised variables are defined as:

$$z^* = \frac{z}{L};\ C^* = \frac{CLK_{av}}{F_{in}};\ t^* = K_{av}t;\ w^* = \frac{w}{K_{av}L};\ s_f{}^* = s_f L;\ \lambda^* = \frac{\lambda}{K_{av}};\ K_E{}^* = \frac{K_E}{K_{av}}$$

The lower layer equations become:

$$\frac{\partial \phi_s}{\partial t^*} = \phi_{s1} s_f{}^* f - K_E{}^* \phi_s - \frac{\partial w^* \phi_s}{\partial z^*} \tag{3.14}$$

$$\frac{\partial \phi_s C^*}{\partial t^*} = \phi_{s1} s_f{}^* f C_1{}^* - K_E{}^* \phi_s C^* - \frac{\partial w^* \phi_s C^*}{\partial z^*} - \lambda^* \phi_s C^* \tag{3.15}$$

The surface layer equations are:

$$\frac{\partial \phi_{s1}}{\partial t^*} = \frac{w_0{}^* \phi_{s0} - w_r{}^* \phi_{s1} - f\phi_{s1}}{z_r{}^*} \tag{3.16}$$

$$\frac{\partial \phi_{s1} C_1{}^*}{\partial t^*} = \frac{w_0{}^* \phi_{s0} C_0{}^* - w_r{}^* \phi_{s1} C_1{}^* - f\phi_{s1} C_1{}^*}{z_r{}^*} - \lambda^* \phi_{s1} C_1{}^* \tag{3.17}$$

The surface boundary conditions are:

$$\phi_{s0} w_0{}^* = \phi_{sE} w_E{}^* + \int_{z_r{}^*}^{1} \phi_s K_E{}^* \, \mathrm{d}z^* \tag{3.18}$$

$$\phi_{s0} w_0{}^* C_0{}^* = \phi_{sE} + \int_{z_r{}^*}^{1} \phi_s K_E{}^* C^* \, \mathrm{d}z^* \tag{3.19}$$

It should be noted that there is scope for temporal variation in many of the functions and parameters. For example, the proportion of infill and collapse, f could be time-varying, as could the excavation and infill functions (K_E and s_f). These possibilities have not been explored in this work.

After making some simplifying assumptions, I derived steady state analytical solutions to these equations. The assumptions are by no means justifiable on biophysical grounds, and are made to allow the convenience of an analytical solution (Mulsow et al. (1998) referred to this as an ostrich-like strategy, and I agree). It is assumed that porosity is constant, that K_E is a constant over all depths, and that surface material is distributed back into the burrow uniformly, so

$$s_f{*} = K_E{*} = \begin{cases} 0, & z{*} \le z_r{*} \\ \dfrac{1}{1-z_r{*}}, & z{*} > z_r{*} \end{cases} \tag{3.20}$$

Constant porosity and steady state assumptions reduce the lower equations to

$$\frac{\partial w{*}}{\partial z{*}} = \frac{f-1}{1-z_r{*}} \tag{3.21}$$

$$\frac{\partial w{*}C{*}}{\partial z{*}} = \frac{fC_1{*} - C{*}}{1-z_r{*}} - \lambda{*}C{*} \tag{3.22}$$

and the surface layer equations become

$$w_0{*} - f - w_r{*} = 0 \tag{3.23}$$

$$\frac{w_0{*}C_0{*} - fC_1{*} - w_r{*}C_1{*}}{z_r{*}} - \lambda{*}C_1{*} = 0 \tag{3.24}$$

and the surface boundary conditions are

$$w_0{*} = w_E{*} + 1 \tag{3.25}$$

$$w_0{*}C_0{*} = 1 + \frac{1}{1-z_r{*}}\int_{z_r{*}}^{1} C{*}\,\mathrm{d}z{*} \tag{3.26}$$

Analytical solutions to these equations are:

$$w_r{*} = w_0{*} - f \tag{3.27}$$

$$w{*} = \frac{w_0{*}(1-z_r{*}) + z_r{*} - f + (f-1)z{*}}{1-z_r{*}} \tag{3.28}$$

$$C^* = \frac{fC_1^*}{f+\lambda^*(1-z_r^*)} + \frac{\lambda^*(1-z_r^*)C_1^*}{f+\lambda^*(1-z_r^*)}\left\{\frac{w_0^*(1-z_r^*)+z_r^*-f+(f-1)z^*}{(w_0^*-f)(1-z_r^*)}\right\}^{\frac{f+\lambda^*(1-z_r^*)}{1-f}} \quad \textbf{(3.29)}$$

$$C_1^* = \frac{1}{A_1}\left[1-\frac{f}{A_1A_2}+\frac{\lambda^*(1-z_r^*)A_3}{A_1A_2(1+\lambda^*(1-z_r^*))}\left\{\left(\frac{w_0^*-1}{A_3}\right)^{\frac{1+\lambda^*(1-z_r^*)}{1-f}}-1\right\}\right]^{-1} \quad \textbf{(3.30)}$$

where

$$A_1 = w_0^* + \lambda^* z_r^*$$
$$A_2 = f + \lambda^*(1-z_r^*)$$
$$A_3 = w_0^* - f$$

These solutions are valid for $0 \le f < 1$. f = 0 represents the collapse-only case (which is equivalent to an upward conveyor belt model with uniform removal with depth), and f = 1 represents the infill only case (which is equivalent to Boudreau's burrow-and-fill model). The analytical solution for $f = 1$ needs to be derived separately.

For $f = 1$ the lower layer equations are:

$$\frac{\partial w^*}{\partial z^*} = 0 \quad \textbf{(3.31)}$$

$$\frac{\partial w^* C^*}{\partial z^*} = \frac{C_1^* - C^*}{1-z_r^*} - \lambda^* C^* \quad \textbf{(3.32)}$$

and the surface layer equations are:

$$w_0^* - 1 - w_r^* = 0 \quad \textbf{(3.33)}$$

$$\frac{w_0^* C_0^* - C_1^* - w_r^* C_1^*}{z_r^*} - \lambda^* C_1^* = 0 \quad \textbf{(3.34)}$$

If the sedimentation velocity is zero, the analytical solution is simply two layers of uniform concentration. The lower layer tracer concentration is

$$C^* = \frac{C_1^*}{1+(1-z_r^*)\lambda^*} \tag{3.35}$$

and the upper layer tracer concentration is

$$C_1^* = \left[\frac{(1+\lambda^* z_r^*)(1+(1-z_r^*)\lambda^*)-1}{1+(1-z_r^*)\lambda^*}\right]^{-1} \tag{3.36}$$

For a non-zero sedimentation velocity, the analytical solution is:

$$C^* = \frac{C_1^*}{1+(1-z_r^*)\lambda^*}\left[1-\lambda^*(1-z_r^*)\exp\left\{-\frac{(z^*-z_r^*)(1+(1-z_r^*)\lambda^*)}{w_E^*(1-z_r^*)}\right\}\right] \tag{3.37}$$

$$C_1^* = \left[\begin{array}{l} w_0^* + \lambda^* z_r^* - \dfrac{1}{1+\lambda^*(1-z_r^*)} \\ + \dfrac{\lambda^*(1-z_r^*)w_E^*}{(1+(1-z_r^*)\lambda^*)^2}\left(\exp\left\{-\dfrac{(1+(1-z_r^*)\lambda^*)}{w_E^*}\right\}-1\right)\end{array}\right]^{-1} \tag{3.38}$$

I constructed a numerical version of the model (equations (3.14) to (3.19)) using the method of lines in Matlab. The advection terms were discretised using an upwind differencing scheme, and Matlab's stiff ordinary differential equation integrator, 'ode15s' was used to integrate the resulting ordinary differential equation. There was excellent agreement between numerical solutions and the analytical solutions (visually indistinguishable). The numerical model is used in Section 3.4.3 to model more complicated porosity and excavation assumptions.

3.3 *Physical interpretation and typical behaviour*

3.3.1 Effect of parameter values in the EIC model

The key parameters in the EIC model are z_r^*, f, λ^* and w_E^*. The non-dimensional thickness of the surface uniformly mixed layer is given by z_r^*. f represents the relative magnitude of infill compared with excavation. λ^* represents the relative magnitude of decay compared with excavation rate. The normalised sedimentation rate w_E^*

represents the relative magnitude of the sedimentation rate compared with excavation. The relative influence of each of these processes is illustrated in the following examples.

The effects of varying f can be seen in Figure 3.2 for $w_E^* = 0.1$, $\lambda^* = 1$ and $z_r^* = 0.1$. The burrowing zone is located in the region $0.1 < z^* < 1$. Beneath the burrowing zone tracers are subject to decay and burial only. For $f = 0$ (collapse only), the tracer profile decreases linearly from the surface mixed layer. For $f = 1$ (infill only), the tracer profile decays rapidly to a relatively high constant value which persists to the base of the burrowing zone. Surface material is being directly injected uniformly with depth to the base of the burrowing layer in this case, so it is not surprising that relatively high concentrations are seen at depth. The $f = 0.5$ profile (equal amounts of collapse and infill) generally lies between the two extremes of the $f = 0$ and $f = 1$ case. Below the base of the burrowing zone at $z^* = 1$ the tracer is subject only to natural sedimentation velocity and decay.

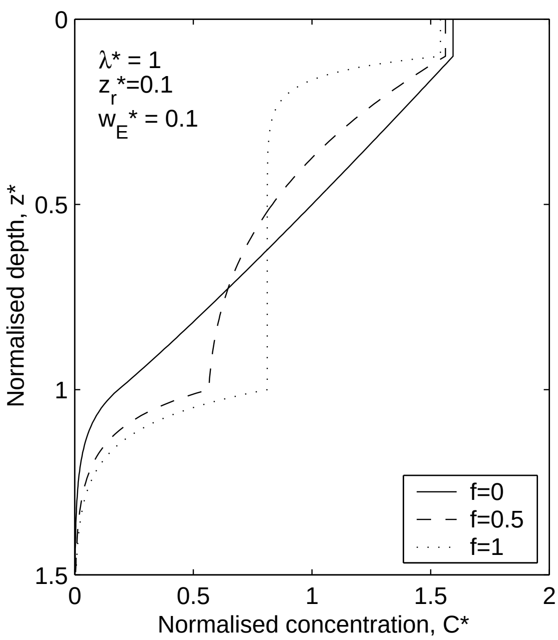

Figure 3.2 Comparison between EIC model solutions with different f values.

Increasing w_E^* has the effect of reducing the differences between the three models (Figure 3.3). This would suggest that in areas where the natural sedimentation rate is high, quantifying the relative amounts of burrow collapse and infill would appear to be unimportant.

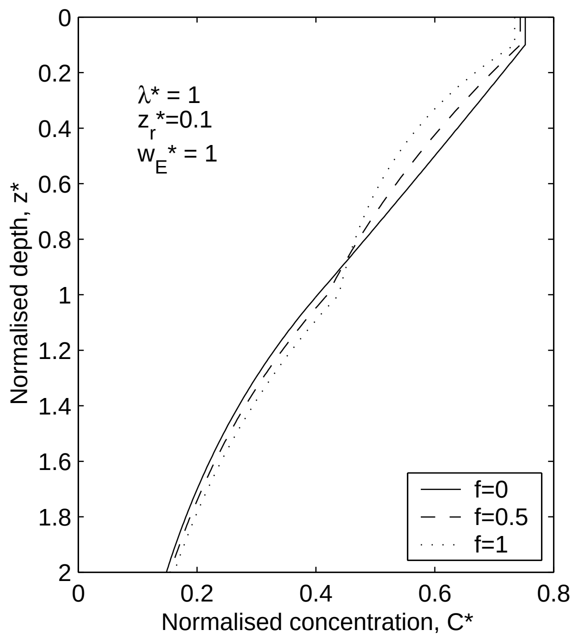

Figure 3.3 EIC model solutions with the same parameters as Figure 3.2, except $w_E = 1$.

Decreasing w_E* to zero maximises the differences between the three models (Figure 3.4). Note that the $f = 1$ profile is simply a three-layer profile. There is a surface peak overlying a uniformly mixed sediment column to the base of the burrowing zone, and no tracer is transported below the base of the burrowing zone. Clearly, if sediment turnover due to bioturbation is so high that natural sedimentation rates are negligible, the specific mechanisms for exchange play a more important role in determining the shape of tracer profiles.

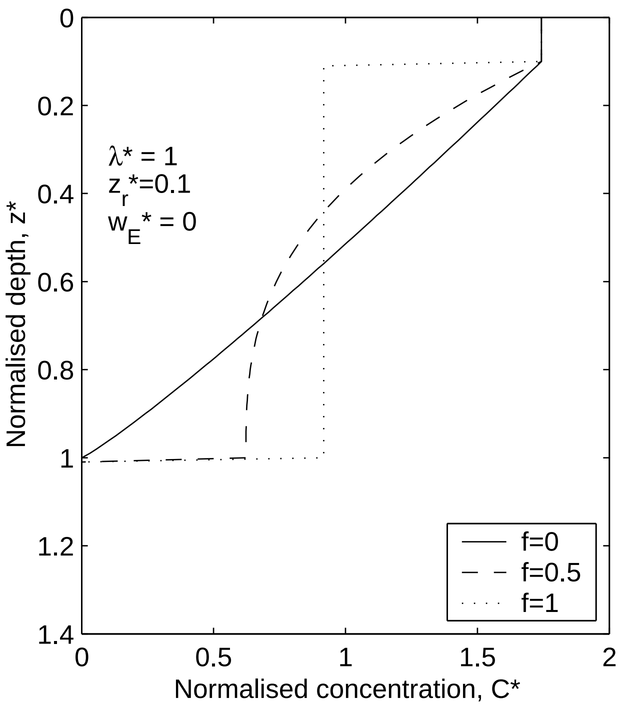

Figure 3.4 Model solutions with the same parameters as Figure 3.2, except $w_E = 0$.

3.3.2 Comparison between the EIC and diffusion models

For the purposes of comparison, the diffusion model can be formulated in a similar framework to the EIC model by assuming that there is a uniformly mixed surface layer of thickness z_r overlying a burrowing zone (with biodiffusion coefficient D_b) extending to depth L. The sedimentation rate is w_E and the material flux at the surface is F_{in}. Again, constant porosity is assumed.

Non-dimensionalising in a similar manner to before (although D_b is used instead of K_{av})

$$z^* = \frac{z}{L}; C^* = \frac{CD_b}{LF_{in}}; t^* = \frac{D_b t}{L^2}; w^* = \frac{wL}{D_b}; \lambda^* = \frac{\lambda L^2}{D_b}$$

The governing equation (non-dimensionalised, steady state) for the burrowing zone is

$$\frac{\mathrm{d}^2 C^*}{\mathrm{d}z^{*2}} - w_E{}^* \frac{\mathrm{d}C^*}{\mathrm{d}z^*} - \lambda^* C^* = 0 \tag{3.39}$$

For the inventory, $I = \int_0^\infty C \, \mathrm{d}z$ to be at steady state, the incoming flux balances the loss due to decay so forming one condition that must be met when solving equation (3.39).

$$\begin{aligned}
&\frac{\mathrm{d}I}{\mathrm{d}t} = F_{in} - \lambda I = 0 \\
&\Rightarrow \lambda \int_0^\infty C \, \mathrm{d}z = F_{in} \\
&\Rightarrow \lambda^* \int_0^\infty C^* \, \mathrm{d}z^* = 1
\end{aligned} \qquad \textbf{(3.40)}$$

Another condition at steady state is that the diffusive flux out of the uniformly mixed surface layer needs to balance remaining material fluxes in this layer (surface flux entering the layer, decay and advection out of the layer). The condition is expressed in the following equation

$$1 - \lambda^* C_1^* z_r^* - w_E^* C_1^* + \left.\frac{\mathrm{d}C^*}{\mathrm{d}z^*}\right|_{z_r^*} = 0 \qquad \textbf{(3.41)}$$

Other conditions are that concentrations need to be continuous at boundaries between layers (ie. at $z^* = z_r^*$ and $z^* = 1$). The analytical solution equations describing the diffusion model profiles are then

$$C^* = \begin{cases} A\exp\left(\beta_1 z_r^*\right) + B\exp\left(\beta_2 z_r^*\right) & z^* \le z_r^* \\ A\exp(\beta_1 z^*) + B\exp(\beta_2 z^*) & z_r^* < z^* \le 1 \\ \left[A\exp(\beta_1) + B\exp(\beta_2)\right]\exp\left\{-\dfrac{\lambda^*}{w_E^*}(z^* - 1)\right\} & z^* > 1 \end{cases} \qquad \textbf{(3.42)}$$

where

$$\begin{aligned}
&A = \frac{1-\gamma_2}{\gamma_1} B; \qquad B = \frac{\gamma_1 + \alpha_1 \lambda^*}{(\gamma_1 \alpha_2 - \gamma_2 \alpha_1)\lambda^*} \\
&\gamma_1 = \beta_1 - \lambda^* z_r^* - w_E^*; \qquad \gamma_2 = \beta_2 - \lambda^* z_r^* - w_E^* \\
&\alpha_1 = \left(z_r^* - \frac{1}{\beta_1}\right)\exp\left(\beta_1 z_r^*\right) + \left(\frac{1}{\beta_1} + \frac{w_E^*}{\lambda^*}\right)\exp(\beta_1) \\
&\alpha_2 = \left(z_r^* - \frac{1}{\beta_2}\right)\exp\left(\beta_2 z_r^*\right) + \left(\frac{1}{\beta_2} + \frac{w_E^*}{\lambda^*}\right)\exp(\beta_2) \\
&\beta_1 = \frac{w_E^* + \sqrt{{w_E^*}^2 + 4\lambda^*}}{2}; \qquad \beta_2 = \frac{w_E^* - \sqrt{{w_E^*}^2 + 4\lambda^*}}{2}
\end{aligned}$$

For the purposes of comparison, the following examples have been converted back to dimensional variables. Selected fixed values of L, z_r, F_{in}, λ, K_{av}, f and w_E were used and then values of D_b were found that produce the best diffusion model match to the EIC-generated profile (while retaining the same L, z_r, F_{in} and λ values), and vice versa.

Figure 3.5 illustrates an example that is the equivalent to the scenario in Figure 3.2 ($\lambda^* = 1$, $w_E^* = 0.1$, $z_r^* = 0.1$, $f = 0.5$ in the EIC model). Values of $L = 70$ cm, $F_{in} = 1$ and $\lambda = 0.031$ y^{-1} were chosen (so $K_{av} = 0.031$ y^{-1}). The value of D_b that provides the closest match to the EIC model (least squares difference between the two profiles) is $D_b = 40.0$ cm^2y^{-1}.

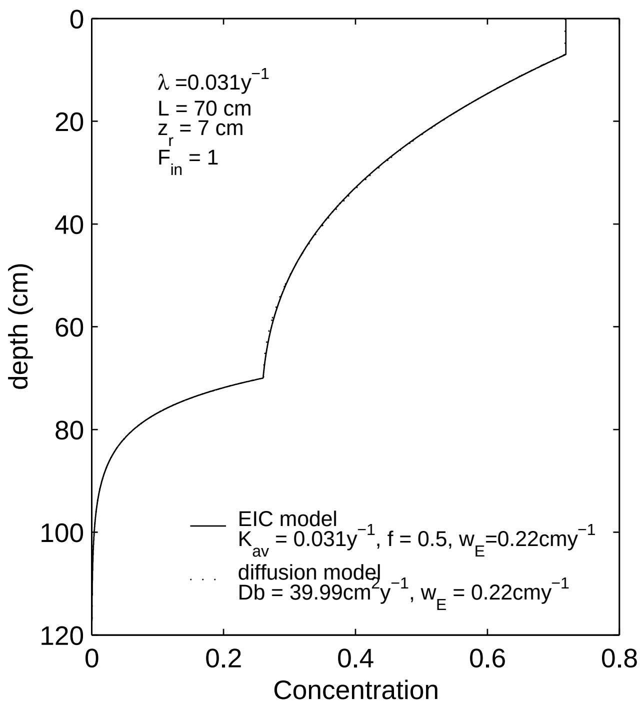

Figure 3.5 Comparison between EIC and diffusion model profiles. The EIC model parameters are the same as those in Figure 3.2 ($f = 0.5$ case), and diffusion model parameters have been found to produce the least squares difference between the two models.

The two profiles in Figure 3.5 are indistinguishable, which agrees with Boudreau's comment that similar profiles can be generated from very different processes. For other parameter values, however, the match is not so close. In Figure 3.6(a) the value of λ^* for the EIC model is increased to 5 (so the corresponding value of K_{av} is 0.0062) and the value of . In this example the diffusion model provides a relatively poor match; in particular the non-zero values at depth resulting from surface material infill cannot be simulated using a diffusion approach. In this case I forced the diffusion model to use the 'correct' sedimentation velocity, w_E = 0.043 cm/yr. If w_E is allowed to vary, the match is no better (Figure 3.6(b)).

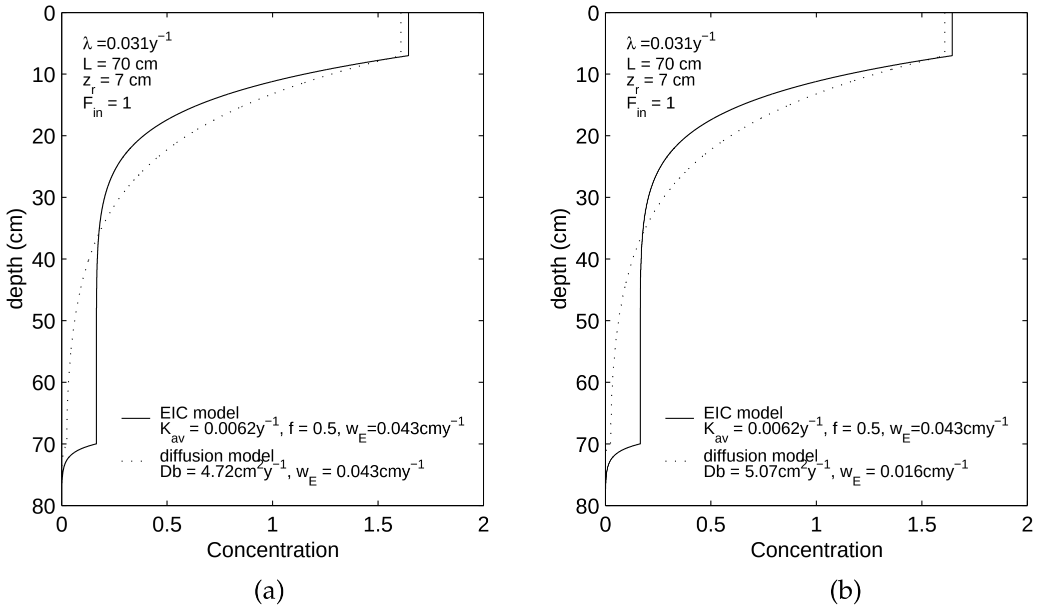

Figure 3.6 Two diffusion model fits to EIC model profiles: (a) the diffusion model has been forced to use the same sedimentation velocity as the EIC model; (b) all diffusion model parameters are allowed to vary to fit the EIC model profile.

The differences are further accentuated if *f* is closer to 1 in the EIC model, as illustrated in Figure 3.7. The diffusion model is unable to produce a profile that is generated by such a high level of infill from the surface.

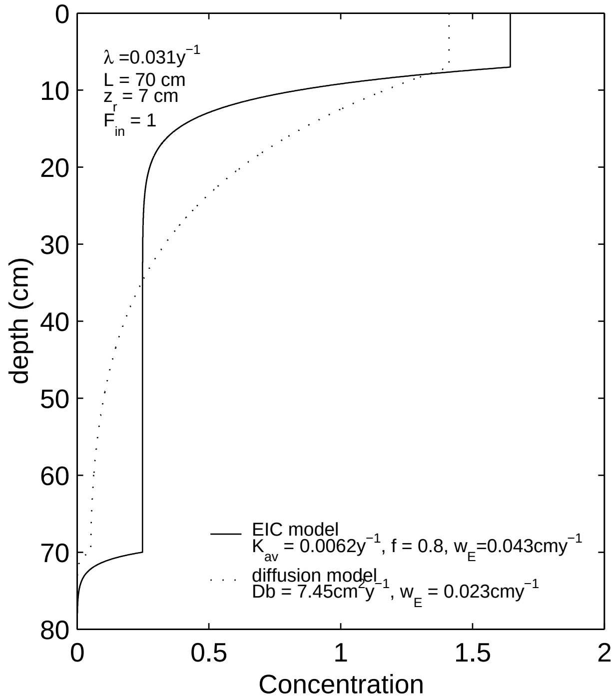

Figure 3.7 Comparison between EIC and diffusion model profiles. EIC model parameters are the same as in Figure 3.6, with the exception of *f* which has been increased to 0.8.

The comparison of the diffusion and EIC models demonstrates that the EIC model produces a more diverse range of profile shapes. While some of its profiles are very similar to diffusion profiles, it is capable of generating a range of profiles that cannot be mimicked by a diffusion model (Figure 3.7).

The EIC model presented here has one more parameter than a similar formulation of the diffusion model, so it is not surprising that it is able to produce a greater variety of profile shapes. It is important to determine whether the extra model complexity (the inclusion of another parameter) provides enough of an improvement for it to be considered a 'better' model. The next section uses a maximum likelihood approach to applying and testing the EIC model, including making the comparison with the diffusion model.

3.4 *Case study: Port Phillip Bay ^{210}Pb and ^{228}Th profiles*

3.4.1 Problem description and parameter estimation method

Hancock and Hunter (1999) used excess ^{210}Pb and ^{228}Th profiles to quantify sedimentation and bioturbation rates in Port Phillip Bay (PPB). ^{210}Pb has a half-life of 22.3 years. It is generated in the sediments (the 'supported' ^{210}Pb) and also arrives at the sediment surface (the 'excess' ^{210}Pb). The excess ^{210}Pb is fallout from the atmosphere, and it is scavenged by particles in the water column which then deposit on the sediment surface. The depositional flux of ^{210}Pb is usually assumed to be constant over time. ^{228}Th has a half-life of 1.9 years. It is generated in the water column, where is it scavenged by suspended sediment and deposited on the sediment surface. It is generated in the sediment also. Again the excess ^{228}Th is used, and it is assumed to be a constant depositional flux. All ^{210}Pb and ^{228}Th data referred to in this chapter are the excess concentrations.

Hancock and Hunter (1999) employed an advection diffusion equation with two unknown parameters, the sedimentation rate and the biodiffusion coefficient. As there were profiles from two tracers of different half lives, a least squares fit to the profile pairs could be used to determine the two parameters.

The cores were taken from three sites within Port Phillip Bay, and the core names were SC1, FS1, SC3, LC3 and SC2 (short core 1, frozen slab core 1, short core 3, long core 3 and short core 2). The numbers refer to the site location (sites 1 and 3 were located in the centre of the Bay, and site 2 was in the far north of the Bay). In this work modelling has been restricted to the cores from sites 1 and 3 because the porosity variation with depth at site 2 was much higher than in the other sites (0.34 to 0.77 at site 2, compared with 0.72 to 0.87 at sites 1 and 3). The analytical solution to the EIC model requires constant porosity, an assumption that is violated in all cores, but most severely in SC2 and so this core is excluded from the analysis. Mulsow et al. (1998) pointed out that it's not the variation in porosity that matters, so much as the variation in solid fraction. Although there is a large difference between the ratios of highest/lowest porosity (1.2 for sites 1 and 3 compared to 2.3 for SC2), the ratios of the highest/lowest solid fractions are closer (2.2 for sites 1 and 3 compared to 2.9 for SC2), so it may have been valid to include SC2 in my analysis.

Hancock and Hunter (1999) determined the slope of the profiles plotted in log-linear space. They observed three distinct layers of different slope in the profiles: a fairly uniform surface layer (Layer 1, ~2 cm thick) overlying two layers of differing slope (Layer 2 between 2 cm and 20 cm and Layer 3 between 21 cm and 45 cm). The slopes were shallowest in Layer 3, and the biodiffusion coefficient calculated for this lowest layer exceeded the biodiffusion coefficient determined for Layer 2 by a factor of between 2.5 and 10. The authors commented that this result goes against expectations; biodiffusion coefficients are expected to decrease with depth, reflecting the reduced density of animals. Their explanation for their seemingly anomalous result was that burrowing shrimps and worms inhabit PPB sediments to depths exceeding 40 cm. These animals' activities could allow rapid transport of surface material to depth (either through inverse conveyor feeding or infilling of vacant tunnels). This observation suggests that the EIC model may be more appropriate for modelling the PPB sediment profiles.

There were a number of assumptions embedded in the analysis by Hancock and Hunter (1999). They split the profiles into three layers for analysis, choosing the section boundaries by eye. This effectively fixed the parameters L and z_r. They made no assumptions about F_{in} as they only fitted the slopes of the curve in log-space. However, to match the core profiles (and not just slopes) their D_b and w_E values would need to be combined with estimates of F_{in}. So while they only estimated two parameters (D_b and w_E), their results fixed particular values of L, z_r and F_{in}. Thus there were effectively five parameters in their system. The EIC model requires one more parameter, replacing D_b with f and K_{av}.

A further comment about estimating F_{in} values: where a sediment core is sufficiently long, F_{in} can be estimated well from the inventory and λ for each tracer. Only one core (LC3) was deep enough to do this, leaving much greater uncertainty in F_{in} for the other cores.

Rather than analysing the profiles by layer, as Hancock and Hunter (1999) did, I used the above formulations of the diffusion and EIC models to model the whole profile. Parameters were fitted using a maximum likelihood approach (Hilborn and Mangel (1997)) and 90% confidence intervals were found for all parameters.

Following Hilborn and Mangel (1997), the likelihood of the data given the hypothesis is expressed as

$\mathcal{L}\{\text{data} \mid \text{hypothesis}\}$

and the negative log-likelihood is

$\mathbf{L}\{\text{data} \mid \text{hypothesis}\} = -\log(\mathcal{L}\{\text{data} \mid \text{hypothesis}\})$.

The likelihood of the data given the hypothesis is assumed to be proportional to the probability of the data given the hypothesis (and is further assumed to be identical, without loss of generality). This form of analysis requires the hypotheses under test to be stochastic models, however the EIC and diffusion models have been presented as deterministic models only. I assumed that the set of observed tracer concentrations, C_{obs} depend on the deterministic values, C_{det} (the values predicted by the EIC or diffusion model) and the measurement uncertainty U:

$$C_{obs} = C_{det} + U \tag{3.43}$$

It follows that the probability distribution for the difference between the observed and deterministic values (C_{obs} - C_{det}) is the same as the probability distribution for U. The tracer counts are Poisson distributed, and the standard deviation for each data point (σ_i) is known. As counts are high, the Poisson distribution can be well approximated by a Normal distribution. Consequently, in the likelihood estimation procedure I assumed that U is Normally distributed. The negative log-likelihood for the i^{th} data point is then the log of the Normal distribution function:

$$\mathbf{L}_i = \ln(\sigma_i) + \frac{1}{2}\ln(2\pi) + \frac{\left[C_{obs,i} - C_{det,i}\right]^2}{2\sigma_i^2} \tag{3.44}$$

and the negative log-likelihood for a tracer profile containing n points is:

$$\mathbf{L} = \sum_{i=1}^{n} \left\{ \ln(\sigma_i) + \frac{1}{2}\ln(2\pi) + \frac{\left[C_{obs,i} - C_{det,i}\right]^2}{2\sigma_i^2} \right\} \tag{3.45}$$

The set of parameters that minimises equation (3.45) are those that provide the closest fit between the model and the observed data. (Note that if σ_i were the same for all i, this approach would yield the same set of parameters as a least squares fit). The advantage of the negative log-likelihood approach is that the values of **L** can be used to construct likelihood profiles (defined below) and prescribed confidence intervals on the parameter values.

The MLE (maximum likelihood estimate) can be used to compare different models with differing numbers of parameters, so allowing a comparison of the EIC model with the diffusion model. The EIC model has one more parameter than the diffusion model, so we need to ensure that any improved fit is not simply due to the addition of one more parameter.

Model parameters for each core were estimated using Matlab's 'fminsearch' function, using all the observed ^{210}Pb and ^{228}Th data for that core. This is an unconstrained nonlinear optimisation function which uses the simplex search method, and it was applied to find the parameters that minimise the value of **L**. An unconstrained optimisation function is not ideal, as in this system there are constraints on all parameters (eg. all parameters have to be nonzero). To include these constraints in the optimisation routine, transformed parameters were used (for example, squaring parameters to ensure positive values, or mapping to a sin function to ensure they remained within a desired range). I limited L to a range of 40 – 80 cm, w_E to a range of 0 – 0.5 cm/yr and allowed z_r to be no greater than 30% of the profile depth. The ^{210}Pb and ^{228}Th profiles were fitted together.

Another common problem with optimisation routines is their tendency to dwell in local minima as global minima are notoriously difficult to locate, and results are likely to be sensitive to the initial parameter 'guesses' supplied to the optimisation routine. This problem was addressed by conducting hundreds of optimisations (>500) starting from randomly chosen starting points.

Once model parameters had been estimated for a core, likelihood profiles were constructed for each parameter, which is a form of sensitivity analysis. One parameter was fixed at a particular value, and the remaining parameters were estimated using the optimisation routine. The fixed parameter was then changed to another value and the process repeated. Where the resulting plot of **L** against the fixed parameter range is a steeply-sided U-shape, the parameter is well constrained; a flat curve indicates that the observed data are insufficient to estimate the parameter well.

Quantified confidence bounds can be derived from the likelihood profiles using the likelihood ratio test. If $\mathcal{L}_1$ is the maximum likelihood value when all parameters are allowed to vary, and $\mathcal{L}_0$ is the maximum likelihood value when one value has been fixed and the others allowed to vary, $\chi^2 = -2\ln(\mathcal{L}_0/\mathcal{L}_1)$ has an approximate Chi-Square distribution with one degree of freedom. When we convert to negative log-likelihoods, $\chi^2 = 2(\mathbf{L}_0 - \mathbf{L}_1)$. So, for example, at the 90% confidence boundaries $\mathbf{L}_0 = \mathbf{L}_1 + 1.35$.

3.4.2 Results of Maximum Likelihood analysis

Example likelihood profiles are presented in Figure 3.8. Solid lines are the likelihood profiles and dashed lines indicate the negative log-likelihood value corresponding to

90% confidence for each model (1.35 above the minimum negative log-likelihood value). The 90% confidence bounds are the intersection points between the likelihood profile and the dashed line associated with that profile. An example of a well-constrained parameter is the ^{210}Pb flux value estimated for SC1 by the diffusion model (90% confidence bounds of 7.4 and 8.1 mBq/cm^2/yr). At the other extreme, the maximum burrow depth, *L*, is poorly constrained by the data, and values ranging from 42.5 cm to 80 cm are all equally likely for the EIC model. Another important observation is that the two models can make quite different predictions about a parameter. For example, for LC3 the diffusion model estimates a lower limit of 0.32 cm/yr for the sedimentation velocity (with 0.46 cm/yr as the most likely estimate), whereas the EIC model for the same data estimates a range of 0.08 cm/yr to 0.32 cm/yr (with 0.18 cm/yr as the most likely estimate).

The confidence bounds for all parameters and all cores are given in Table 3.1 to Table 3.4. The 90% confidence ranges were much broader than I had expected, and in many cases the data were unable to infer very much about the parameters values at all. Hancock and Hunter (1999) calculated a diffusion coefficient of 5.0 ± 0.1 cm^2/yr and a sedimentation velocity of 0 – 0.15 cm/yr for the 2-20 cm region of sediment. Extending the diffusion analysis to the full profile and conducting a more rigorous uncertainty analysis produced a far greater range of diffusion coefficients and sedimentation velocities. Viable D_b estimates range from 1.0 – 16 cm^2/yr, and sedimentation velocities range from 0 – 0.5 cm/yr.

Sedimentation velocity had to be manually constrained to 0.5 cm/yr; in the absence of this constraint, even higher sedimentation velocities would fall within the 90% confidence range (regardless of model choice). This imposed constraint can be justified on the grounds that the depositional flux in the bay was calculated to be 0.42 cm/yr, which would be an over-estimate as it includes re-suspended sediment (Hancock and Hunter (1999)). The core data were therefore inadequate to estimate the sedimentation velocity in most cases.

The results underline the need to capture the full profile in a sediment core. LC3 was the only core deep enough to reasonably constrain estimates of *L* and ^{210}Pb F_{in} in the EIC model. The incoming flux estimates can only be estimated well when the full tracer inventory is captured by the core. LC3 was also different in that the estimates for z_r were much higher than in the other cores (up to 20 cm, compared with up to 5.9 cm for other cores). These values are arguably too high, as it is physically unrealistic to have uniform, instant mixing to depths of 20 cm. I re-ran the parameter estimation scripts with a constraint that $z_r < 10$ cm in LC3, however the negative log-likelihood values were far higher, and visual inspection of the core plainly shows uniform mixing to this depth. The original report providing the ^{210}Pb and ^{228}Th data (Hancock et al. (1997)) stated that LC3 was a longer and narrower core than the others and that the top 10-20cm may have been artificially mixed during core collection and freezing. Given this knowledge, good information about the mixing behaviour in LC3 cannot be inferred; however it remains a valuable core as it is the only one that captures the full ^{210}Pb inventory.

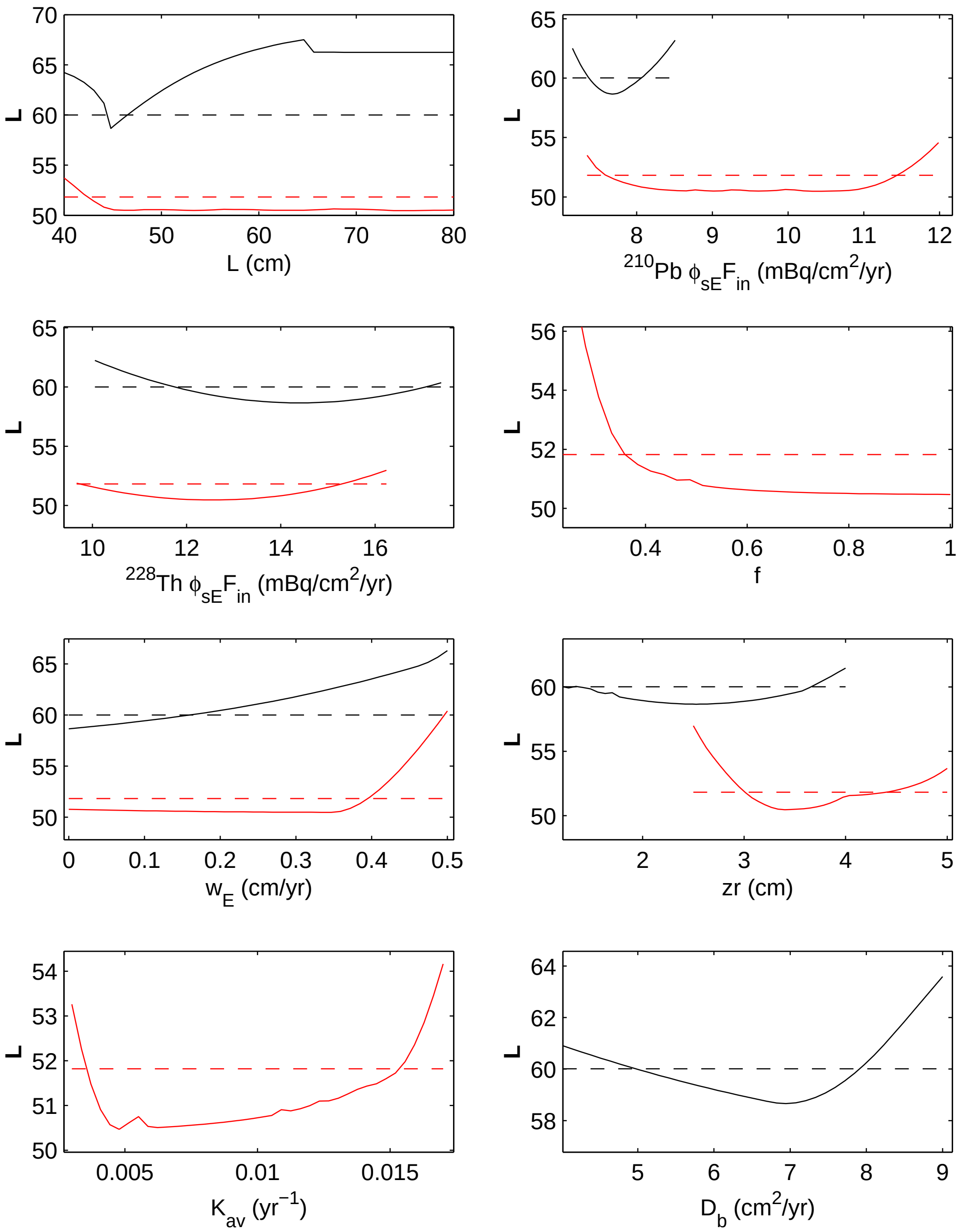

Figure 3.8 Likelihood profiles for EIC and diffusion model fits to SC1 data. Solid lines are the likelihood profiles and dashed lines indicate the negative log-likelihood value corresponding to 90% confidence for each model (1.35 above the minimum negative log-likelihood value). The red plots are results from the EIC model and the black plots are results from the diffusion model.

Table 3.1 Parameter estimates and 90% confidence intervals for EIC and diffusion model fits to SC1 core data.

	EIC model			Diffusion model		
Parameter	**Best fit**	**90% lower bound**	**90% upper bound**	**Best fit**	**90% lower bound**	**90% upper bound**
L (cm)	74.5	42.5	80	44.8	44.6	46.5
^{210}Pb $\phi_{SE}F_{in}$ (mBq/cm^2/yr)	10.4	7.6	11.4	7.7	7.4	8.1
^{228}Th $\phi_{SE}F_{in}$ (mBq/cm^2/yr)	12.5	9.7	15.3	14.4	11.7	17.1
f	1.00	0.36	1	-	-	-
w_E (cm/yr)	0.35	0	0.39	0	0	0.16
z_r (cm)	3.4	3.0	4.4	1.8	1.2	3.7
K_{av} (yr^{-1})	0.0048	0.0036	0.015	-	-	-
D_b (cm^2/yr)	-	-	-	6.9	5.0	7.9

Table 3.2 Parameter estimates and 90% confidence intervals for EIC and diffusion model fits to FS1 core data.

	EIC model			Diffusion model		
Parameter	**Best fit**	**90% lower bound**	**90% upper bound**	**Best fit**	**90% lower bound**	**90% upper bound**
L (cm)	41.7	40	80	40	40	80
^{210}Pb $\phi_{SE}F_{in}$ (mBq/cm^2/yr)	8.3	7.7	12.6	8.8	7.8	9.5
^{228}Th $\phi_{SE}F_{in}$ (mBq/cm^2/yr)	22.3	16.1	28.2	20.8	15.5	26.0
f	0.39	0.27	1	-	-	-
w_E (cm/yr)	0.0	0	0.50	0.43	0.0	0.50
z_r (cm)	4.3	3.5	5.9	3.7	2.1	4.9
K_{av} (yr^{-1})	0.020	0.0014	0.024	-	-	-
D_b (cm^2/yr)	-	-	-	1.7	1	8.0

Table 3.3 Parameter estimates and 90% confidence intervals for EIC and diffusion model fits to SC3 core data.

	EIC model			Diffusion model		
Parameter	**Best fit**	**90% lower bound**	**90% upper bound**	**Best fit**	**90% lower bound**	**90% upper bound**
L (cm)	60.5	42.3	80	43.3	42.6	45
^{210}Pb $\phi_{SE}F_{in}$ (mBq/cm^2/yr)	12.1	8.4	15.1	8.4	8.1	10.1
^{228}Th $\phi_{SE}F_{in}$ (mBq/cm^2/yr)	15.3	11.5	20.3	16.9	14.2	19.7
f	0.99	0.54	1	-	-	-
w_E (cm/yr)	0.44	0	0.5	0	0	0.5
z_r (cm)	2.6	2.1	3.2	2	2	2.4
K_{av} (yr^{-1})	0.013	0.010	0.027	-	-	-
D_b (cm^2/yr)	-	-	-	14.1	7.3	16.0

Table 3.4 Parameter estimates and 90% confidence intervals for EIC and diffusion model fits to LC3 data.

	EIC model			Diffusion model		
Parameter	**Best fit**	**90% lower bound**	**90% upper bound**	**Best fit**	**90% lower bound**	**90% upper bound**
L (cm)	52.8	48.9	57.2	45	41.3	80
^{210}Pb $\phi_{SE}F_{in}$ ($mBq/cm^2/yr$)	11.9	11.1	12.6	11.8	11.0	12.6
^{228}Th $\phi_{SE}F_{in}$ ($mBq/cm^2/yr$)	25.7	12.1	35.5	24.1	12.0	35.5
f	1.00	0.75	1	-	-	-
w_E (cm/yr)	0.18	0.08	0.32	0.46	0.32	0.5
z_r (cm)	19.4	16.7	20	13.3	10.3	15.8
K_{av} (yr^{-1})	0.0087	0.0067	0.013	-	-	-
D_b (cm^2/yr)	-	-	-	3.6	1.7	3.1

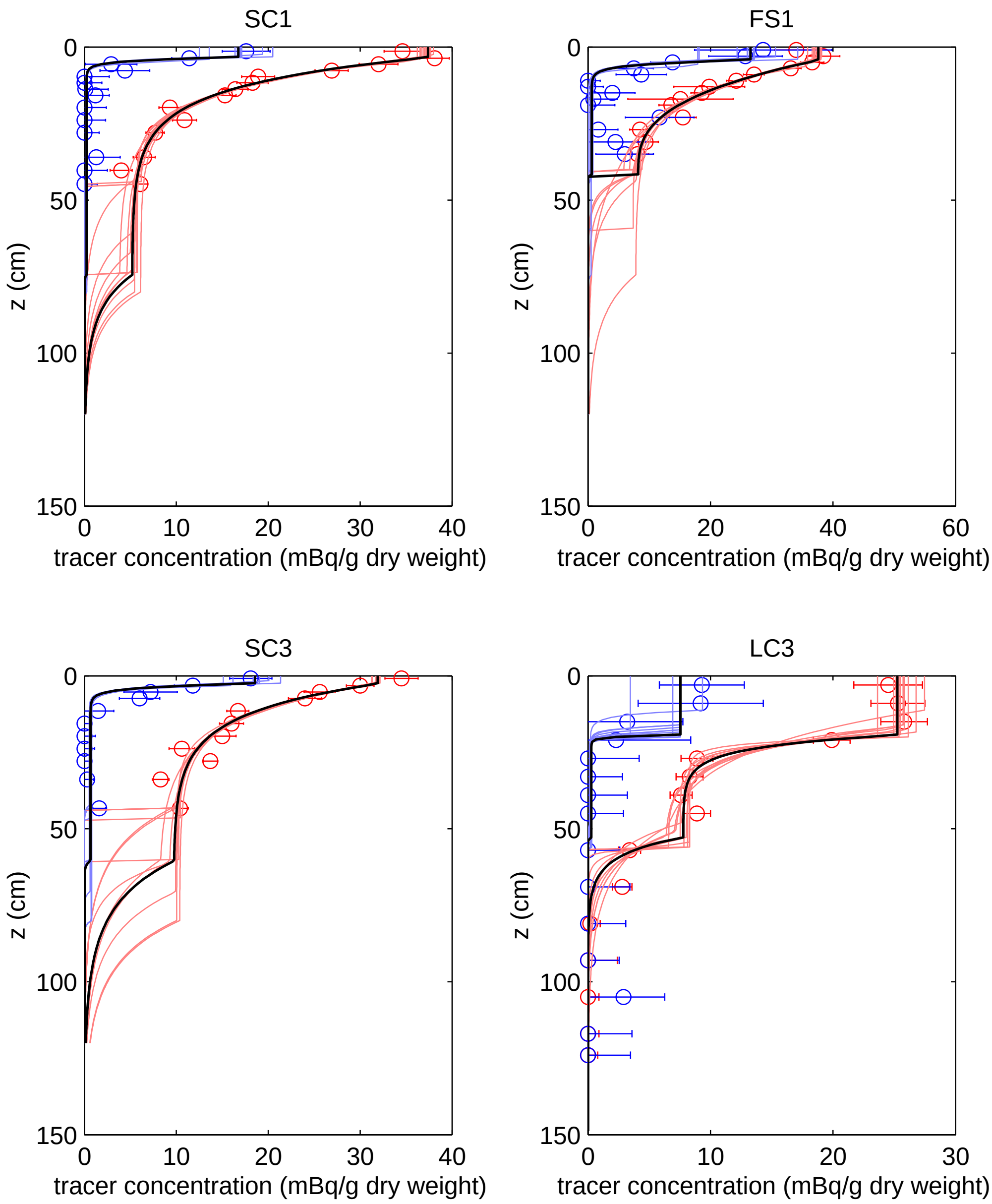

Figure 3.9 EIC model fits to core data. Red markers are ^{210}Pb data, blue markers are ^{228}Th data. Black lines are the best model fits to the data. The lighter red and blue lines demonstrate a range of possible fits constructed from parameters values lying at the extremes of the 90% confidence bounds.

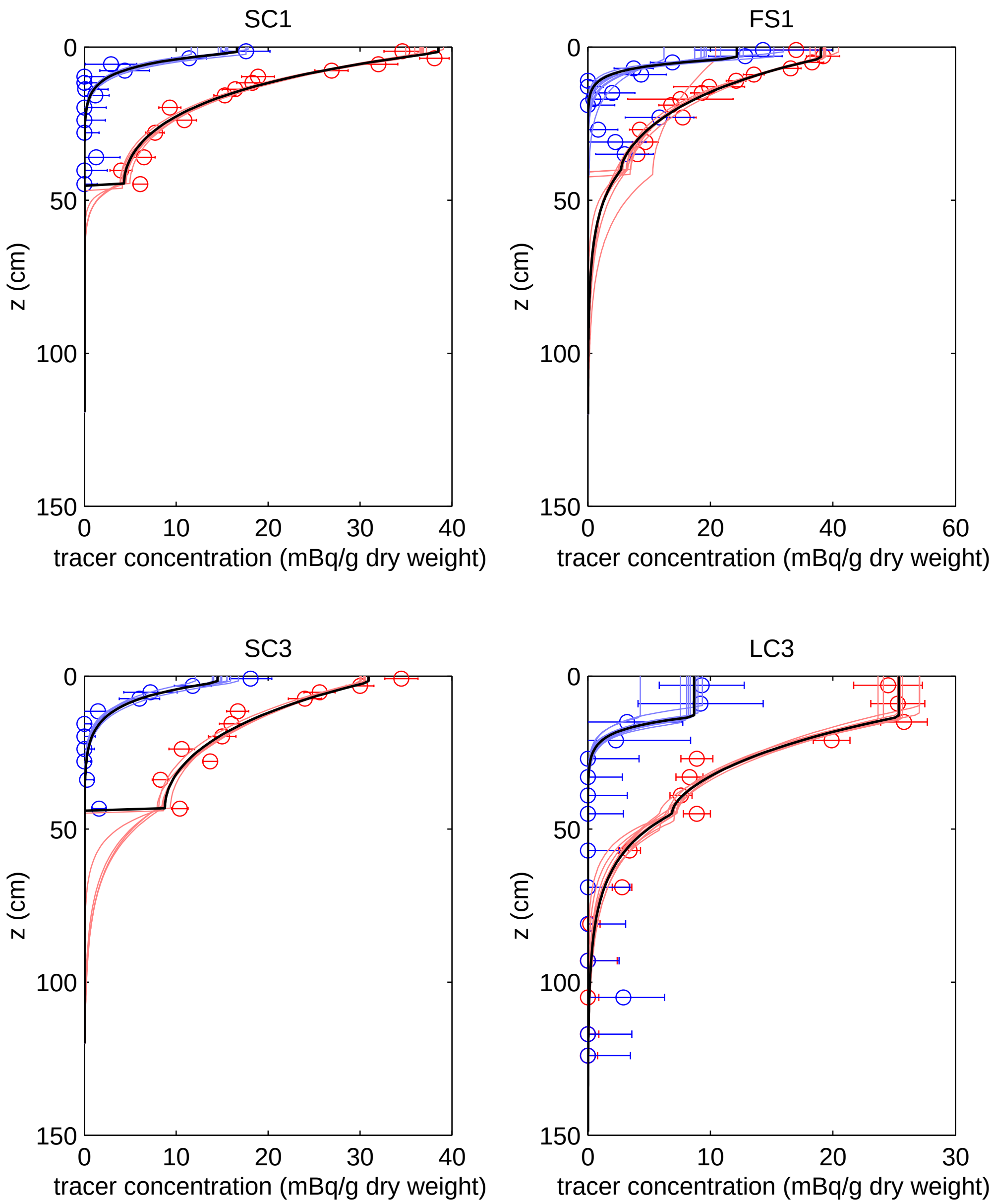

Figure 3.10 Diffusion model fits to core data. Markers and line colours are the same as in Figure 3.9.

The EIC model fits have been plotted against the data in Figure 3.9 and the diffusion model fits in Figure 3.10. Included in these plots are model fits that lie at the extremes of the 90% confidence parameter range. The aim of this figure is to demonstrate visually that the wide ranges calculated for parameters really do produce viable fits to the data (a visual check on the more formal likelihood calculations). Figure 3.9 demonstrates the drawbacks of short cores quite clearly. There is a large range of possible EIC model concentrations at depths greater than the deepest measured point for all cores other than LC3. Another point to note is the impact of the range of sedimentation velocity values on profile shape. For example, in the EIC model fits for SC3 we can see some profiles exhibit a sharp concentration drop to zero at the base of the burrowing zone (indicating w_E is close to or at zero) while other profiles are characterised by a more gradual decrease to zero below the burrowing zone (indicating a much higher w_E).

For all cores the EIC model fits produced a higher maximum likelihood value, so by this measure, provided a better fit to the data. Whether the improvement is significant or not can be judged using the Akaike Information Criterion (AIC), A_i, for comparing non-nested models. This criterion adds a penalty for each additional parameter. The AIC for model M_i with p_i parameters is:

$$A_i = 2\mathrm{L}\left(Y|M_i^*\right) + 2p_i \qquad \textbf{(3.46)}$$

where Y is the data and $\mathbf{L}(Y\,|\,M_i^*)$ is the minimum value of the negative log-likelihood evaluated at the best choice of parameters for model M_i (Hilborn and Mangel (1997), with printing error corrected). The best model is the one with the lowest AIC. The AIC values for each core and model are listed in Table 3.5, and demonstrate that in each case the EIC model's improvement in fit is significant for all cores except FS1, where effectively neither model is better than the other.

Table 3.5 AIC values calculated for each core and model using equation (3.46).

Core	EIC Model AIC	Diffusion model AIC
SC1	114.9	129.3
FS1	148.0	147.6
SC3	101.4	111.5
LC3	126.5	135.9

An advantage of the EIC model is that even this simplest version relies on parameters that have a physical meaning, and are measurable. The rate of volume expelled to the surface per unit area, Q_{ex} is simply

$$Q_{ex} = K_{av}L \qquad \textbf{(3.47)}$$

The estimates for Q_{ex} for each core are 0.36, 0.82, 0.78 and 0.46 cm^3/cm^2/year (SC1, FS1, SC3 and LC3 respectively). The laser scanner experiments in Chapter 2 suggested excavation rates of the order of 1 cm^3/burrow opening/day. At this rate, densities of 10 - 24 openings/m^2 would yield the Q_{ex} values inferred from the cores. For the purposes of comparison, actual thalassinidean shrimp densities in PPB ranged from 10 - 21 individuals/m^2 in 1995 (Bird et al. (1997)). Assuming two openings per individual, this corresponds to 20 – 42 openings/m^2. A direct comparison is not strictly valid, as the measurements in Chapter 2 were of a considerably larger species, *Trypaea australiensis*. *Trypaea australiensis* exists within Port Phillip Bay, but is far less common than smaller thalassinidean shrimp species. Nevertheless, the comparison serves to demonstrate that the proposed mixing mechanism and rates are consistent with measured excavation rates from a related species.

The laboratory measurements suggested that burrow infill rates were comparable to sediment expulsions rates, which implies that $f \sim 1$. While $f = 1$ was the best estimate for SC1, SC3 and LC3 and in all cases, f=1 lay within the 90% confidence bounds, f was generally poorly constrained in the maximum likelihood analysis. Even so, the lower bound was never greater than 0.27, indicating that some infill was always needed to provide the best fit.

3.4.3 Model Assumptions

In this section I address the simplifying assumptions made to allow an analytical solution to the EIC model. The assumptions were: uniform constant excavation and infill, steady state conditions and constant porosity. These assumptions greatly reduced the number of parameters which could be varied in the model; there was no option to change depth dependence, non-steady state solutions and different porosity assumptions. The data are too sparse even to constrain the remaining parameters very well, so there is certainly insufficient data to resolve even further detailed inclusions in the model structure. However, there is still merit in experimenting with different model structures to provide an idea of the latitude in these sediment transport descriptions. The numerical version of the EIC model requires none of the above assumptions and so allows the investigation of alternative model assumptions.

We firstly consider the steady state assumption. European settlement dramatically altered the land cover in the catchments. Run-off from cleared catchments can be substantially higher than vegetated catchments, and carry more sediment. The assumption of a constant burial velocity with time ignores the possibility of recent spikes of sediment arriving in the Bay following large-scale land clearing. Given that the bulk of the catchment changes happened over a century ago, any ^{210}Pb from that period would have long since decayed, and the existing ^{210}Pb reflects the sediment mixing processes of only the last few decades. Consequently, I've not experimented with such scenarios with the numerical version of the EIC model.

Further steady state assumptions include constant values of f, K_E and s_f over time. These parameters are all likely to be seasonally influenced, but affected also by relatively sudden changes in surrounding conditions. Temporal variations in weather, tidal velocities and disturbances by other animals are likely to create temporally varying excavation and infill characteristics. Long time-scale variations, such as seasonally-imposed changes, are likely to have the greatest impact on model results and could be included in the model, however I did not conduct any model runs to explore these issues.

The constant porosity assumption is clearly violated in all of the cores. When porosity variation is to be included in a diffusion model, a decision has to be made about the nature of the mixing: is it intraphase or interphase mixing (eg. Boudreau (1997))? The EIC model requires no such distinction to be made, however it does of course need equivalent assumptions defining how porosity is altered by the excavation, infill and collapse process. The simplest approach that retains depth-varying porosity information is to assume the porosity profile is invariant with time, so the left hand side of equation (3.8) is set to zero and can be used to solve for w as a function of depth. The best parameter estimates from the analytical solution were applied to the numerical version of the EIC model, together with this additional porosity assumption. The results are plotted with the core data and compared with the best analytical fit in Figure 3.11. While the numerical model profiles fit the data approximately, the negative log-likelihood values calculated from these profiles are substantially higher than the values for the analytical version. Differences from minimum negative log-likelihood values calculated previously were 5, 4, 33 and 7 for SC1, FS1, SC3 and LC3 respectively (note that a difference of 1.35 was used to calculate 90% confidence boundaries).

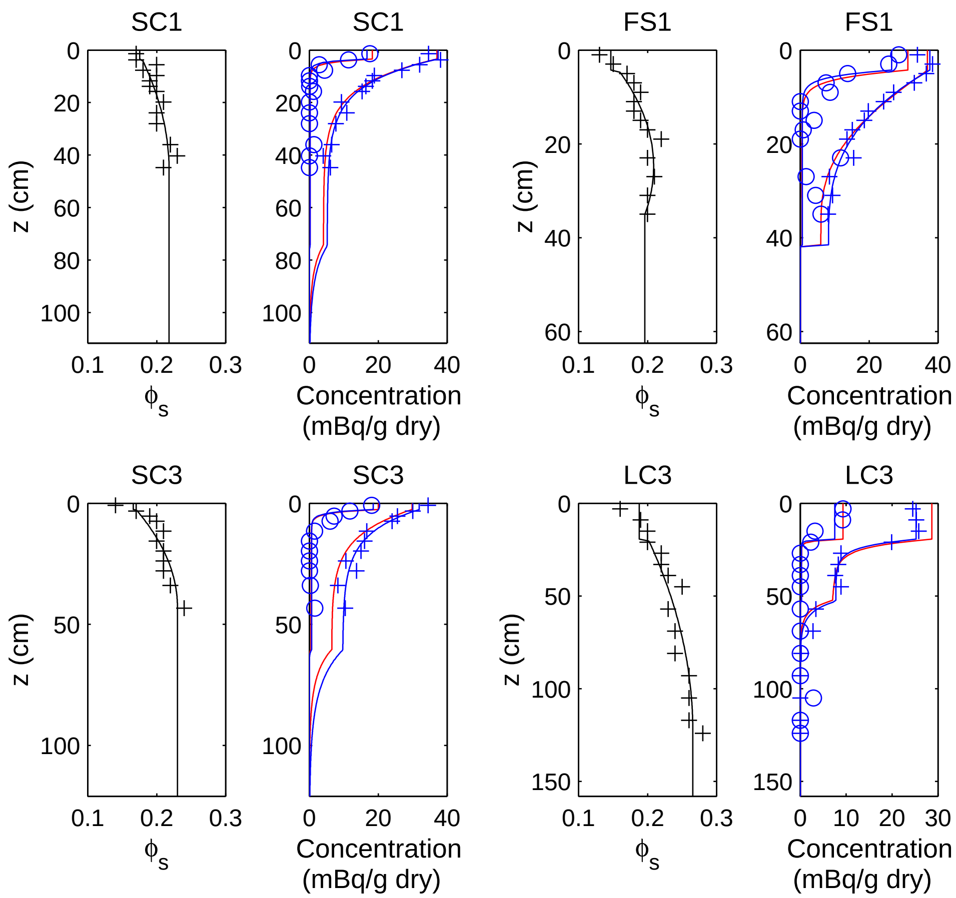

Figure 3.11 Comparison between analytical EIC model best fits (which assume constant porosity), and the numerical model (which assumes a time-invariant depth-varying porosity profile) results if the same parameters are applied. The porosity profiles for each core are shown, along with the quadratic fit used to represent porosity variation in the numerical model. The blue lines are the analytical model best fits and the red lines are the numerical model profiles. The difference in negative log-likelihood values between the two profiles are 5, 4, 33 and 7 for SC1, FS1, SC3 and LC3 respectively.

Uniform burrowing and infill with depth (constant K_E and s_f) is another large assumption underlying this work. Clearly this assumption is physically implausible. It would be relatively easy to use more detailed field data to supply more realistic burrow volumes as a function of depth. To demonstrate the potential impact of such a change, the best parameter estimates from the analytical model were substituted into a numerical version of the EIC model with a linearly decreasing excavation and infill rate (decreasing to zero at the base of the burrowing zone, $z = L$). The results are plotted in Figure 3.12. Again, the visual comparisons of the data and model results appear reasonable, but the negative log-likelihood values calculated for each profile differ substantially from those for the analytical version (differences of 17, 19, 25 and 13 for cores SC1, FS1, SC3 and LC3 respectively).

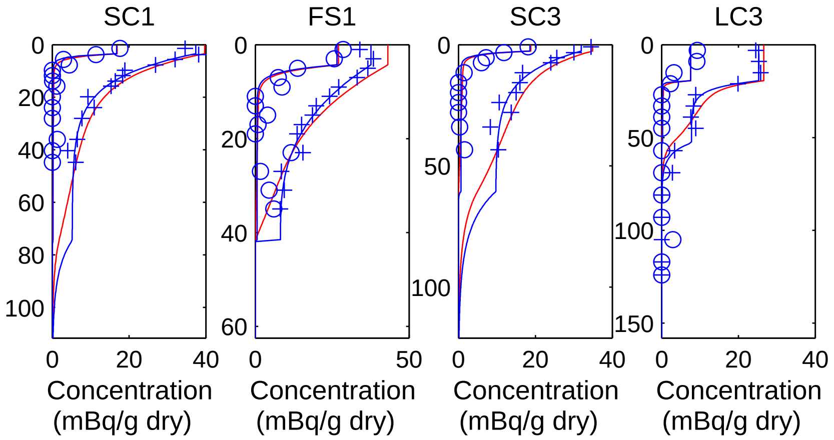

Figure 3.12 Comparison between analytical model best fits (which assume constant porosity and uniform excavation and infill rates with depth), and the numerical model (which assumes constant porosity and linearly decreasing excavation and infill rates with depth) results if the same parameters are applied. The blue lines are the analytical model best fits and the red lines are the numerical model profiles. The difference in negative log-likelihood values between the two profiles are 17, 19, 25 and 13 for SC1, FS1, SC3 and LC3 respectively. Depth axis units are cm.

Parameter confidence bounds were not calculated for either of the above numerical models. The calculations would be considerably more time consuming than for the analytical solution, as tens of thousands of model runs are required and numerical model solutions are substantially slower to calculate than analytical model solutions. If such calculations were to be conducted, new sets of best parameter estimates and confidence bounds would be found. The various sets of best parameters generated from different model assumptions (analytical model; numerical depth-varying porosity model; and numerical depth-varying excavation and infill model) would differ and the model producing the lowest overall negative log-likelihood value would 'win' a competition between these models (as each model contains the same number of parameters). Whether the confidence intervals should be calculated from within the 'winning' model only, or calculated from negative log-likelihood values across all models, is a more difficult question. The conservative approach would be to choose the latter option. It is unclear how such an analysis would alter the existing calculated confidence bounds, although given the large differences in negative log-likelihood values for the model profiles presented in Figure 3.11 and Figure 3.12, the potential increase in parameter bounds is enormous. Certainly the best fits to the two numerical models will produce different parameter sets to the set calculated from the analytical model.

A final comment needs to be made about the representation of uncertainty in the stochastic model. In equation (3.43) the uncertainty term, U, was taken to be the measurement uncertainty based on Poisson distributed counting data. This is not the only source of uncertainty in the model, as there is uncertainty about the mixing process itself. Hence the confidence bounds on error estimates have been calculated from the idealised assumption of measurement uncertainty only, and would be broader if measures of process uncertainty were to be included.

3.5 Conclusions

The EIC model developed here has been shown to be a good alternative to the diffusion model as it can produce similarly-shaped profiles yet its parameters (burrow excavation and infill rates) have more physical meaning than a biodiffusion coefficient. The EIC model is particularly suitable for modelling sediment with large persistent burrows, such as those created by thalassinidean shrimp. The model contains one more parameter than a diffusion equation (D_b is replaced by K_{av} and f), but a maximum likelihood parameter estimation approach allows a formal comparison between the two models using the Akaike Information Criterion (AIC). Such an approach can determine if a better fit by the EIC model is due to the extra parameter or to the model itself.

The EIC and diffusion models were applied to ^{210}Pb and ^{228}Th cores from Port Phillip Bay, where thalassinidean shrimp are known to be important bioturbators. This established that the EIC model gave a better fit to the data for all but one core (where the models performed equally well). The diffusion modelling approach is particularly suspect for PPB cores, as much of the data suggests a substantially higher D_b at depth than at shallower locations. While the EIC model was able to give a better fit to the data, little information on the mixing parameter ranges could be gleaned from the model results. The parameter estimates were poorly constrained, as demonstrated by a sensitivity analysis. In particular, burial velocities, burrow excavation rates and burrow infill were all subject to large 90% confidence intervals. Further, cores from the same site yielded very different parameter estimates.

It was clear from all cores, however, that some degree of burrow infill was required to produce the best EIC model fits ($f > 0.27$ in all cases). This is strong evidence that non-local downward transport from the sediment surface is an important mechanism. For the bulk of my PhD research I was unaware of the work being carried out by David

Shull (Shull (2001), Shull and Yasuda (2001)), and I read his publications only towards the end of my work. It's interesting to see that we drew similar conclusions about the importance of downwards non-local transport and the need to incorporate it into models. Where I chose a continuum model approach, he developed a discrete transition matrix model.

Hancock and Hunter (1999) suggested that burial velocities and biodiffusion coefficients could be well resolved from pairs of radionuclide profiles with differing decay constants. My analysis using the diffusion models and a maximum likelihood approach to estimate parameters and confidence intervals found that estimates for burial velocity and biodiffusion coefficients were relatively poorly constrained by the data. Nevertheless, the excavation rates inferred from each core were consistent with measured excavation rates reported in Chapter 1.

The analytical solution of the EIC model relies on a number of assumptions. Assumptions about constant porosity and uniform burrowing are unrealistic. The computationally expensive requirements of the maximum likelihood approach favoured analytical solutions to the EIC and diffusion models. The maximum likelihood approach was not repeated for the slower numerical solution. However, best parameter estimates from the constant-porosity analytical versions of the model were applied to variable-porosity and linearly decreasing burrowing numerical versions to assess whether these considerations could be important. While visually the comparisons to data appeared reasonable, the difference was enough to suggest that, were a rigorous statistical approach applied, the confidence intervals for the variable-porosity version could be even larger than those estimated using the analytical model.

A possible approach to decide whether to investigate these assumptions further is to use the analytical model to estimate parameters and quantify confidence bounds. If the confidence bounds prove to be quite tight, it would be worth extending the analysis and going through a more computationally intense process of including different porosity assumptions and excavation and infill functions. In the present case, such extra effort is not warranted as the parameters are relatively poorly constrained by the data.

The EIC model suffers the same problems as any one-dimensional description of a three-dimensional process. In particular, heterogeneity introduced by burrowing is obliterated by the lateral averaging. In the next chapter, the EIC model is extended to two and three dimensions to investigate the impacts of dimensionality.